REGULAR PAPER

Self-powered Flexible PDMS Channel Assisted Discrete Liquid Column Motion Based Triboelectric Nanogenerator (DLC-TENG) as Mechanical Transducer

M. Shahriar[1] · Cong Phat Vo[1] · Kyoung Kwan Ahn[1]

Abstract

Fluid flow in small scale channel as droplet, continuous or discrete volume of liquid has been used in the multidisciplinary research field to be utilized in wide variety of applications in chemistry, biology, medical technologies. Recently, energy scavenging technique that merges the microfluidics with liquid–solid contact electrification charging from the small flows has become a new area of investigation to be applied as sensory module. In this article, a flexible fluid based mechanical sensing element using the triboelectrification of the oscillatory discrete volume of liquid flowing inside the hydrophobic mini channel over PTFE polymeric film is described. To achieve the high output efficiency and to reduce the wettability of the channel, micropatterned PDMS surface was implied for smooth operation and constant power output of the device. Pressure gradient was applied for the forward–backward motion of the liquid column over the free-standing mode porous PTFE thin film-based electrode and a maximum of 10 nA of short circuit current and 20 mV of open circuit voltage was achieved at 40 mbar pressure and frequency of 1 Hz. Finally, the flexible DLC-TENG shows better performance as a transducer to be effectively used in measuring the frequency response to the angular displacement of the rotary actuator consequently pressure fluctuation sensing. The obtained results are promising whereas counting nominal deflection of pressure such as in the robotic manipulator or actuator is regarded as an essential factor.

Keywords PDMS channel · DLC-TENG · PTFE film · DI water · Mechanical transducer

Abbreviations

DLC-TENG	Discrete liquid column triboelectric nanogenerator
PDMS	Polydimethylsiloxane
MA-PDMS	Micro-architectured PDMS
PTFE	Poly tetra-fluoro Ethylene
DI	Deionized water

1 Introduction

The innovation of novel strategies and advanced technologies for self-powered micro/nano systems with durability, eco-friendly, active sensing capabilities is the key realization arena for energy harvesting and still a challenging task for scientist and engineers. To mitigate the dependency on the large-scale power consumption from solar, wind, tidal etc. for powering portable electronics or sensor, energy sources compatible with the size and low power consumption are prerequisite demand. From the last few decades, concentrations are given on developing green techniques to capture wasted but available energy sources in surroundings like human walking, mechanical actuation or vibration, water flowing, movement of hydraulic machinery [1–13]. Apart from many well developed techniques to harvest ambient energy from the environment that are in vogue since the past century such as thermoelectric [14], piezoelectric and pyroelectric energy conversion process [15, 16], streaming potential of continuous flow [17, 18], recently triboelectric approaches [19–21], which have drawn attention to be an attractive candidate for realizing self-powered, cost-effective active transducer for mechanical sensing [22–25], chemical detection [26, 27] etc.

Triboelectric nanogenerator (TENG) comprises of the contact electrification [28, 29] and electrostatic induction. When two dissimilar materials are bought into physical

✉ Kyoung Kwan Ahn
KKahn@ulsan.ac.kr

1 School of Mechanical Engineering, University of Ulsan, 93, Daehak-ro, Nam-gu, Ulsan, Republic of Korea

contact with each other due to electrostatic induction there is a redistribution of charges with the opposite sign on the two surfaces according to tribopolarities. After a while, separation occurs by means of any external mechanical force which induces triboelectricity that can generate a potential drop and drive the electrons to flow between the electrodes attached with the surfaces [30, 31]. TENG has four fundamental modes till now, including, vertical contact-separation mode, lateral sliding mode, singe electrode mode, freestanding sliding mode. In addition, a lot of structures, prototypes and functions have already been reported and are still going on [7, 32, 33].

Mostly triboelectric devices involve solid–solid contact electrification. The charge generation through friction process solely depends on the difference of the ability of the two surfaces to loss or gain electrons. Electrical output can be improved via change of the surface morphological properties in this process [34]. Nevertheless, the performance can be greatly influenced by the air humidity, dust, which causes instability of the output values of the solid–solid TENG without any encapsulation [35]. Also wear abrasion due to physical collision deteriorates the long-term output stability of the TENG. However, liquid–solid contact electrification has demonstrated the capability of stable response with full contact separation process with the counter solid part. The output shows regular behavior for long term application with good wear resistance while using the liquid for contact [36, 37]. In liquid–solid TENG, the liquid can change its shape and mostly work as a positive tribo-material that exhibit feasibility to be used in flexible and wearable sensor applications.

Considering possible advantages of the liquid in TENG application, electricity generation with flow in a small channel has paved the way of micro/nano sensing for delicate measurement of pressure variation, angular displacement in precision engineering and mechanical motion. To achieve the best performance from micro, nano or mini channel based liquid TENG, hydrophobicity as well as slippery channel surface are considerable factors [38]. Slippery channel surface holds for Navier slip condition that allows the highly concentrated ions within the slip plane to be mobile [39, 40]. From this perspective, surface irregularities or micro-roughness or chemical modification can be done to reduce the wetting behavior as well as increasing the air gap in the liquid–solid channel interaction. A lot of studies have done till now regarding channel flow and surface modification in fluid-based TENG. In 2016, Lee et al. developed a micro-fluidic channel for pressure sensing and finger motion monitoring but didn't consider the fact of residual water that can stick to the channel surface. The output current was about 1.62 nA at 11.6 N [41]. Choi et al. investigated on self-powered ion concentration sensor for chemical detection of liquid. In his case, with DI water the current was generated up

to 60 nA from ten microchannels [42]. Kim et al. developed an air slug sensor by periodic injection of air and water in the two different PDMS channels with same cross-sectional area of 2 mm × 1.9 mm; lengths were 18 mm and 36 mm long respectively. In this experiment, 10 cm 0.01 M NaCl solution column was used to create the air gap. The peak to peak current was found 0.331 µA [43]. All the processes described above, though efficient but the fabrication process is expensive and time-consuming. So, an easily viable and inexpensive pathway is needed for the robust application and to replace the conventional sensory module.

In our article, a 3D printed micro-architectured PDMS (MA-PDMS) channel assisted liquid–solid TENG is proposed to measure the angular frequency with a certain amplitude and pressure fluctuation of the rotary actuator by deploying discrete DI water column inside the mini-channel and PTFE porous thin film as the counter solid material. The hydrophobicity of the channel surface satisfies Navier–stokes slip boundary condition and ensures stable output from the oscillation of the water column. The novelty of this free-standing mode TENG includes: (1) Cost-effective and simple approach for fabricating hydrophobic channel; (2) self-powered flexible and portable sensor to replace the conventional expensive measuring device in hydraulics and robotics manipulator, actuating device.

2 Experimental Section

To develop the mini-channel for DLC-TENG, instead of the conventional soft lithography process, we have adopted 3D printing technique to develop the micro structured pattern of the mini-channel on the prepared mold which is more viable and easier process.

3 Materials and Methods

As the solid tribomaterial, porous PTFE thin film with 50 µm thickness was purchased from Good Fellow Material (GFM), Korea. PDMS sylgard-184 elastomer precursor part-A, precursor part-B were purchased from Dow Corning. Double distilled water (DI water) (Ultrapure system from our lab) was used for better understanding the electrical output behavior of solid–liquid interaction phenomena in case of different test conditions. All the chemical substances and working liquids were used as received without any further purification process. To characterize the surface morphology and hydrophobicity FE-SEM was conducted by using a Hitachi cold FE-SEM microscopy which operates at 10 kV and contact angle of DI water was determined by the DSA 100 Goniometer (error 1°) according to the sessile-drop

method with 5 µL droplet (KRUSSG mbh, Hamburg, Germany).

3.1 Fabrication Techniques of the MA-PDMS Channel and DLC-TENG

As PDMS itself is hydrophobic in nature, so to improve the working function as well as hydrophobicity, micro/nano roughness is a considerable factor. The hierarchical surface roughness attributes to create the air gap between the water–solid interface and water can easily slide over the surface if it is used as column or droplet and the phenomena have already reported by many literatures to develop the PDMS based channel [44, 45]. Figure 1 shows the schematic of the detailed procedure from the fabrication of the micropatterned PDMS channel to the development of the DLC-TENG. Whereas the conventional process as depicted in Fig. 1a described in the above literatures to create microstructure based channel involves complicated fabrication process i.e. wafer cleaning and priming, sacrificial layer growth on the Si wafer, photolithography, pattern transfer, photoresist removal, wet etching, removal of the sacrificial layer by dipping into acetone, spin coating of the PDMS, curing and peeling off the patterned channel. On the

contrary, our proposed method only consists of three easy steps to make the patterned channel which is very convenient and inexpensive method. A major advantage of this method is the precision of the pattern replication is improved, as any kind of surfactant coating is not required.

Figure 1b shows the detailed procedure of the mini-channel preparation that utilizes the commercially available Fused deposition modeling 3D printing techniques to develop the desired template. The positive pattern of the channel was first designed with the inventor and then 3D printing technique was used to get the desired positive pattern as a casting template. The channel width and height were kept accordingly at 2.8 mm and 0.8 mm. To create the micro surface roughness in the PDMS microchannel, we utilize the layer thickness and fill factor percentage of the FDM printer. The PLA (Poly Lactic Acid) material from our 3D printer Ultimaker Cura 3 was used in this process. At first, three kinds of template were prepared with the varying layer thicknesses (0.06, 0.15, 0.3 and 0.4) mm. Obviously, the 0.4 mm shows the better performance to generate the surface roughness on the PDMS. So, the layer thickness was set to 0.4 mm and the infill density was counted 50% for the linear infill pattern with the nozzle speed of 150 mm/s. The sample was developed by putting it on the XY plane in layer by layer
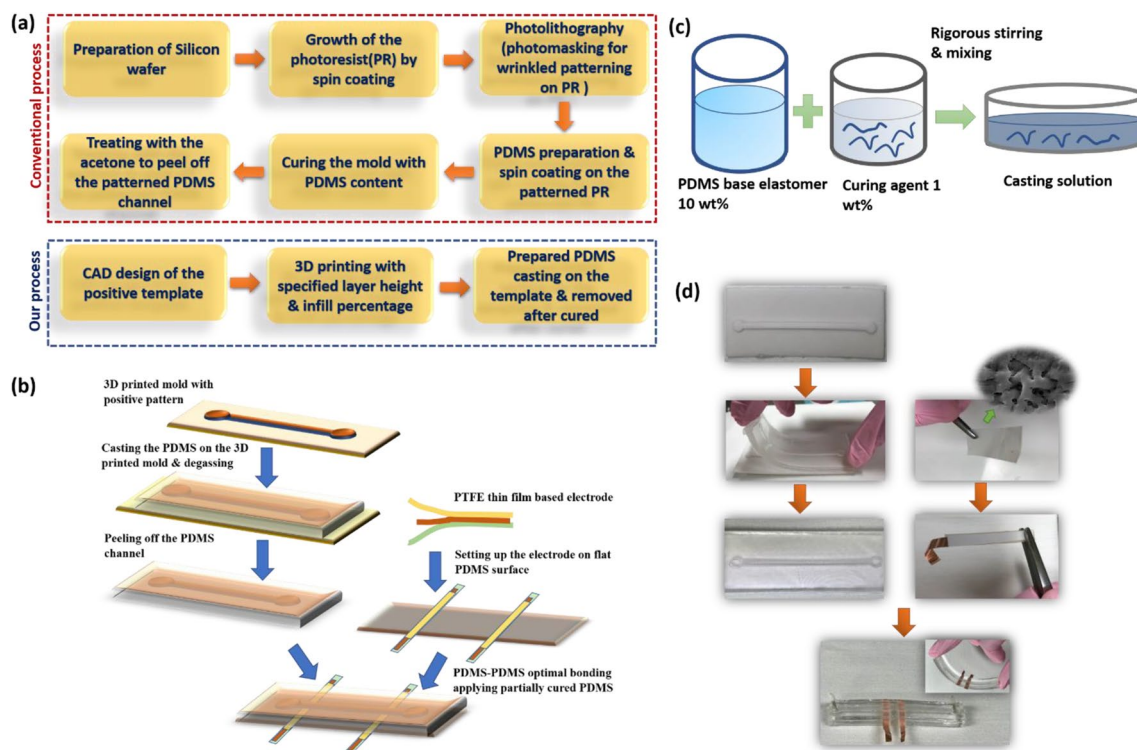
Fig. 1 **a** Difference between conventional process and proposed process to develop the micro structured PDMS channel, **b** preparation of the PDMS casting solution from the base polymer and the curing agent, **c** Schematic diagram showing the fabrication of the PDMS channel, electrode setup on the flat PDMS and PDMS-PDMS bonding. **d** Experimental photograph of the fabrication techniques (Inset: FE-SEM image of the pristine porous PTFE thin film)

formation process. The layer thickness can contribute to the generation of the roughness as reported by Hartcher-O'Brien et al. In the report, the roughness was varied in micro-meter level with the variation in the layer height [46]. For the 0.2 mm layer height, the roughness was found about 35 μm. After preparing the mold to cast the PDMS, at first the mold was rinsed with Iso-propyl alcohol, DI water and then dried in the hot plate for about half an hour. After that, PDMS precursor part-A and precursor part-B were mixed in 10:1 ratio and manually stirred for 10 min to get the uniformly mixed solution, Fig. 1c. Then the solution was casted on the mold pattern and then degassed for 1 h to remove excess air bubbles. After that, the casted PDMS with the mold was kept in the oven at 45 °C overnight. Then, the micro patterned PDMS channel with negative patterning was peeled off from the mold. While peeling off, no mold release material was used that has proved that the adopted procedure is very convenient, viable and reusable. Here, it is noted that, the temperature was kept low, as with the repeated experiment with high temperature it is found that, the polyacrylonitrile plastic shape can be deformed and can damage the proper shape of the PDMS channel. The micro-surface roughness has increased the hydrophobicity of the channel which has discussed in Sect. 2.3.

To obtain the micro-surface roughness based flat PDMS, the same procedure was applied using flat 3D printed mold. PTFE thin film was cut into 2 mm width strip and Cu foil tape was attached on the one side of the film. After that, the adhesive double-sided tape was attached on the bottom side of the Cu foil to complete the electrode making. The Cu foil width was kept nominal smaller than the PTFE film to make ensure the proper sealing to avoid the contact of the Cu foil with the liquid. After peeling off the cured flat PDMS the electrodes are attached on the rough surface.

To complete the fabrication of the DLC-TENG, partially cured PDMS–PDMS bonding technique has been done using PDMS mixture as adhesive [47]. Following this system, PDMS mixture with 10:1 ratio was applied on the patterned surface other than the channel with the scrapping bar. The two-part was then procured at 40 °C for 30 min prior to bonding. After that, both parts gently pushed to each other such that no air bubble is existed and kept in the oven at 60 °C overnight to get fully cured. Two holes with the same size were punched in the two ends and silicon tube was inserted into the hole to complete the fabrication of the DLC -TENG. Figure 1d has represented the real photograph of the development of the proposed TENG.

## 3.2 Surface Morphology Characterization of the PDMS Channel and Porous PTFE Thin Film

Discrete liquid–solid contact electrification involves successive attachment and separation of liquid from the solid surface and therefore net electrical charge is generated. In this context, the solid surface from naturally inspired lotus leaf to triboelectrically sound laboratory developed fluoro-polymer or the polymer treated with silane, protein, etc. should exhibit the hydrophobic property that discrete volume of water can be rolled-off easily from the surface [48]. In our paper, the channel surface with micropatterned roughness facilitates the water column to flow spontaneously without leaving any residuals that satisfy the slip boundary condition $U \neq 0$; in case of mini-channel and effectively increase the uniform output of the electrical performance. Figure 2a shows the FE-SEM images of the regularly patterned linear array of the micro convex curve produced by 3D printing in the inner surface of the PDMS channel which forms the micro air gap between the contact surface and the liquid. The contact angle, depicted in the inset image of the Fig. 2(a), was found 135° for the micro-architectured PDMS channel which proves the obvious hydrophobicity as well as a cost-effective technique to develop the hydrophobic surface. We also checked the FE-SEM and contact angle for the flat PDMS surface produced by 3D printed acrylic plastic material to distinguish the improved performance of MA-PDMS channel. In case of flat PDMS, the contact angle was found 114°. For the development of the flat-PDMS, we have used the acrylic resin based transparent material in the stereolithography (SLA) printer from the central research facility of our university. In this process, the ultraviolet laser guide is passing back and forth according to the input model over the liquid plastic resin supplied from the resin tank and gradually cured it with the increasing temperature. After that, the model has dipped into the acetone to rub off the excess resin. The developed casting template is far smoother than the FDM produced template. Furthermore, the surface characteristics of the micro-porous PTFE thin film that comprises the DLC-TENG cell was analyzed and is shown in Fig. 2c. The micro-porosity with an average pore diameter of 0.866 μm of the commercially bought PTFE thin film produced the contact angle 110.3°. The PTFE thin film has fluorine atoms at both end of long carbon chains which shows excellent water repellency and high electronegativity according to triboelectric series [49].

3.3 Instrumentation for Measuring V_{oc} and I_{sc}

To measure the open circuit voltage and short circuit current, a simple circuit was made by placing a 10 μF capacitor across the two electrodes to get the stable AC output. A Keithley source meter (Keithley Instruments, DMM7510) with the probe resistance value of 10 MΩ was used to measure the V_{oc} and I_{sc}.

Fig. 2 FE-SEM images of **a** the micro-architectured PDMS inner surface; **b** the flat PDMS surface; **c** The porous PTFE thin film. (Inset images are the contact angle of each surface)
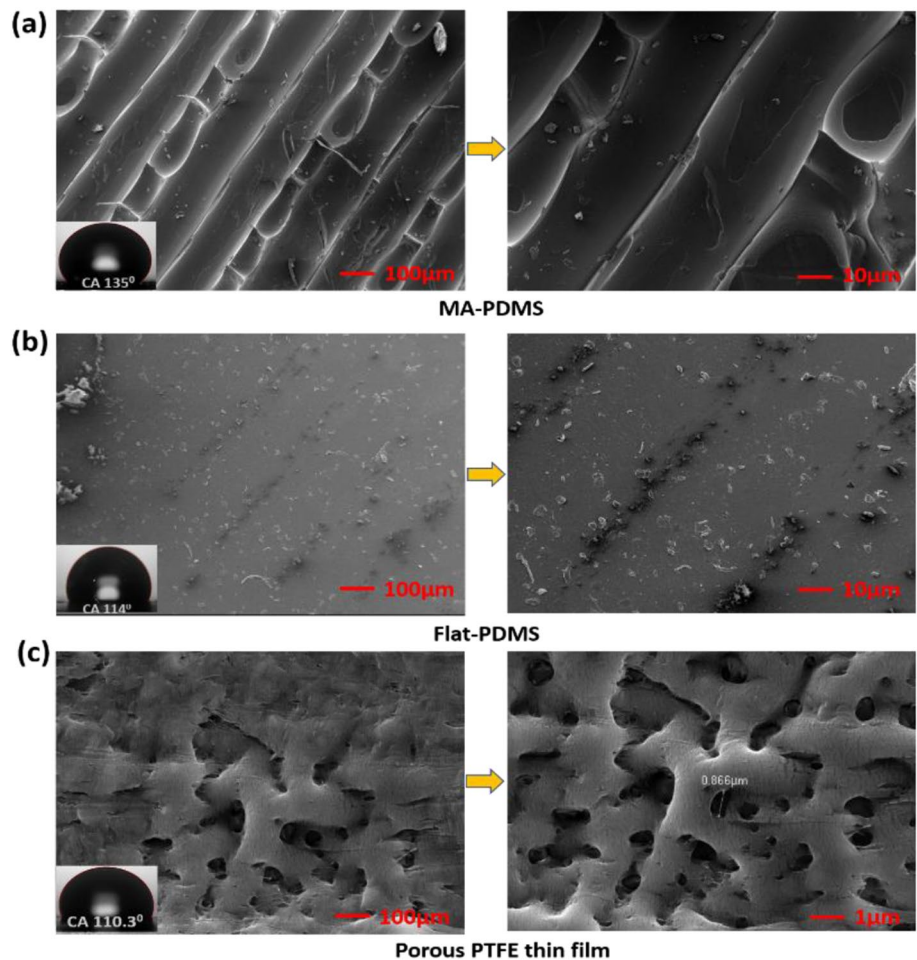
4 Results and Discussion

As shown in Fig. 3a, The DLC-TENG cell is comprised of flexible micropatterned PDMS channel with two microporous PTFE thin film-based electrodes attached inside the channel. The Cu adhesive tapes were shouldered with the copper wire to the capacitor to get the stable and regulated current and voltage signal. For measuring the electrical output of the DLC-TENG, a motion generator was used with controllable frequencies and amplitudes, incorporated by a rotary actuator (SMC-MSQ20A) that generated a pressure gradient for the water column sliding back and forth inside the channel. The actuator consists of a DC motor, adjustable arms connected with the motor shaft and can be synchronized with the frequency response and different amplitude of the pressure provided by the computer-controlled Arduino based IDE as shown in Fig. 3b. The inlet compressed pressure was precisely controlled for different resonance frequency with fixed angular amplitudes ranging from 2.3° to 5.6° and different pressure values to get the desired precise electrical output from the oscillation of the water column inside the MA-PDMS channel.

The detailed working mechanism of the DLC-TENG is described in the Fig. 3c, d and the corresponding AC signal generation is illustrated in Fig. 3e–i during repetitive motion of the liquid column in one cycle. The repetitive back and forth motion of the discrete DI water column over the two PTFE electrodes induces a triboelectric signal following freestanding sliding mode theory. At the steady state, the DI water column is positioned in the PDMS channel other than electrodes. As the PDMS is weakly negative according to the triboelectric series, it increases the positive charge on the surface of the water column by acquiring negative charge itself. When the arm of the rotary actuator moves in the anti-clockwise direction Fig. 3c, the water column moves over the surface of the PTFE thin film of electrode E(1), Fig. 3d. As the PTFE is highly triboelectrically negative, it induces maximum positive tribo-charges on the bottom surface of the water column. So, at the stage (i), the positive charges of the E1 electrode will be neutralized by the excess negative charges of the E2 electrode. When the water column starts approaching to E2 stated by the stage (ii) of Fig. 3d, there is an electrostatic potential difference between E2 and E1
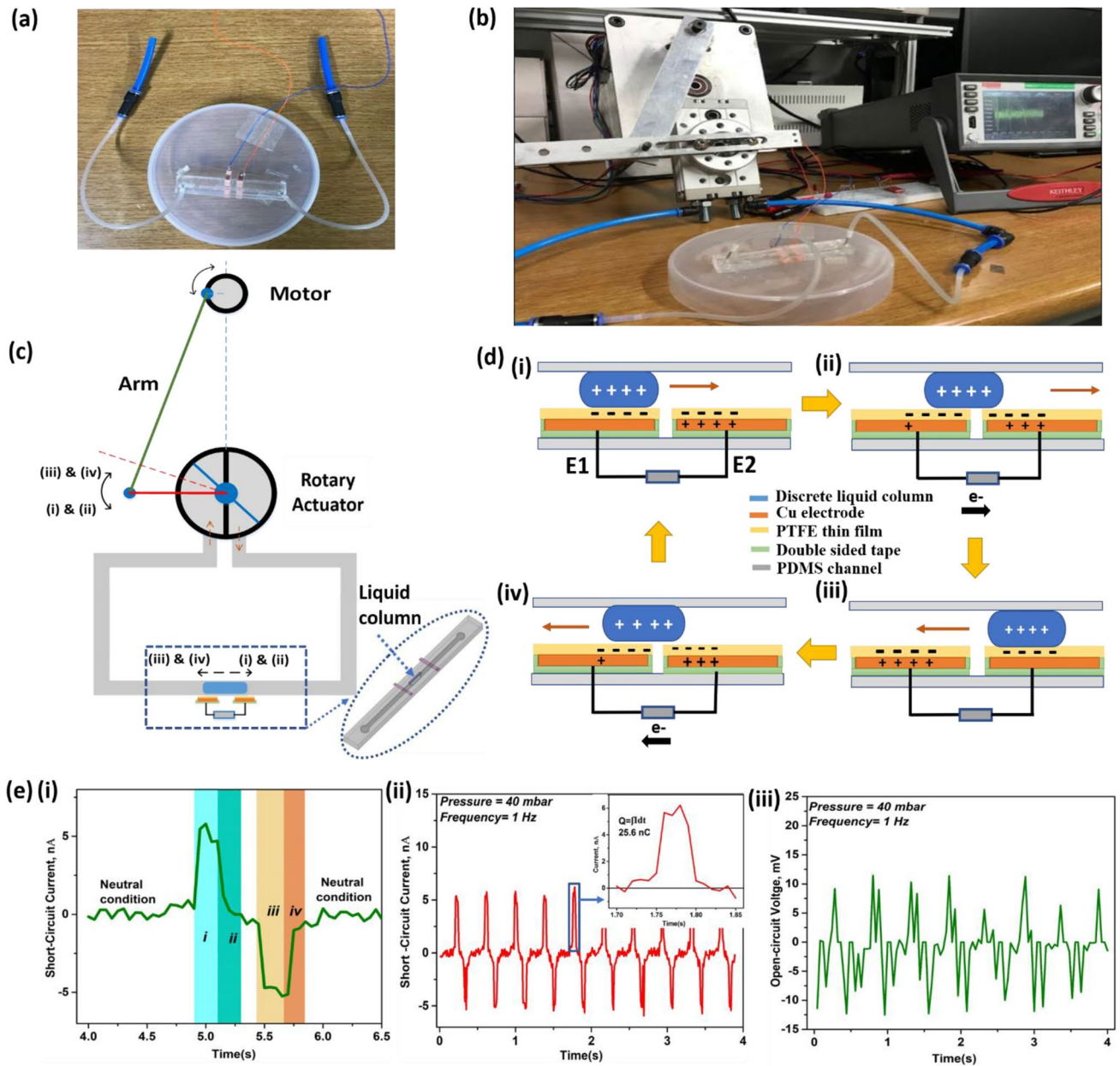
Fig. 3 a Febricated DLC-TENG cell with connecting silicon pipes. **b** Experimental setup of DLC-TENG with the rotary actuator. (Inset image of the Arduino IDE), **c** Schematic diagram to realize the oscillatory motion of DI water column with the angular rotation of the arm. **d** Mechanistic approach for generating V_{oc} and I_{sc} from the free-standing mode DLC-TENG. **e**(i) Magnified view of I_{sc} showing the aforementioned four stages in (c) & (d) that contribute to the AC signal generation in one cycle rotation of the rotary actuator. At the pressure of 40 mbar and 1 Hz (ii) Open circuit voltage, (iii) Short circuit current

that drives the electron to move from E1 to E2. During stage (iii), the water column fully covers the PTFE film of the E2 electrode so thus the Al electrode becomes fully neutralized by the excess release of the electrons from the E1 electrode. After a while, the rotary arm starts to move in the clockwise direction as described in the Fig. 3c. So at the stage (iv) of Fig. 3d, the water column tends to approach towards the E1 electrode causing electrostatic imbalance again and increasing potential is diminished

by the electron flow from the E2 to E1. Thus, the water column reaches at the stage (i) causing the repetition of another cycle. Figure 3e (i) shows the consecutive positive–negative peak of short circuit current of a single oscillation of liquid column that is compatible with the charge generation behavior during the clockwise and anti-clockwise movement of the rotary actuator. During the anti-clockwise direction, positive peak comes out with respect to the E1 electrode and continuously peak is decreasing

with the water column leaving the electrode, the negative peak with the clockwise direction of the actuator denotes the water column is situated over the E2 electrode and continuously reaching the equilibrium state after completely covering the E1 electrode. The phenomenon indicates that the measured output data are in line with the agreement of the predicted theoretical AC behavior as reported in the previous kinds of literature.

The quantitative performance of the DLC-TENG was evaluated to show the effective performance of this simply fabricated device for active sensing of pressure fluctuation and frequency of the rotary oscillator. For this, 2.5 ml of DI water was injected in the channel to generate the oscillation motion in the channel. Figure 3e, (ii), (iii) show the short

circuit current and open circuit voltage at the pressure of 40 mbar and frequency of 1 Hz. The DLC-TENG generates peak to peak open-circuit voltage and short circuit current up to 11.82 nA and 23.2 mV respectively without the additional power supply. Furthermore, under different frequency cycle of specific pressure gradient, both the open circuit voltage and short circuit current show considerably concurrent signal over sequential measurements.

The output performance of the DLC-TENG was characterized by the behavior of the current and voltage output under difference frequency cycle of the rotary oscillator maintaining fixed pressure with definite amplitude and variable pressure gradients. In case of frequency response behavior of the AC signal output, the pressure profile was


Fig. 4 Short circuit current and open circuit voltage at different oscillation frequency of the **a**, **b**, at different pressure gradient **c**, **d**, respectively. **e** Induced coulomb charge for different frequency at the pressure of 40 mbar
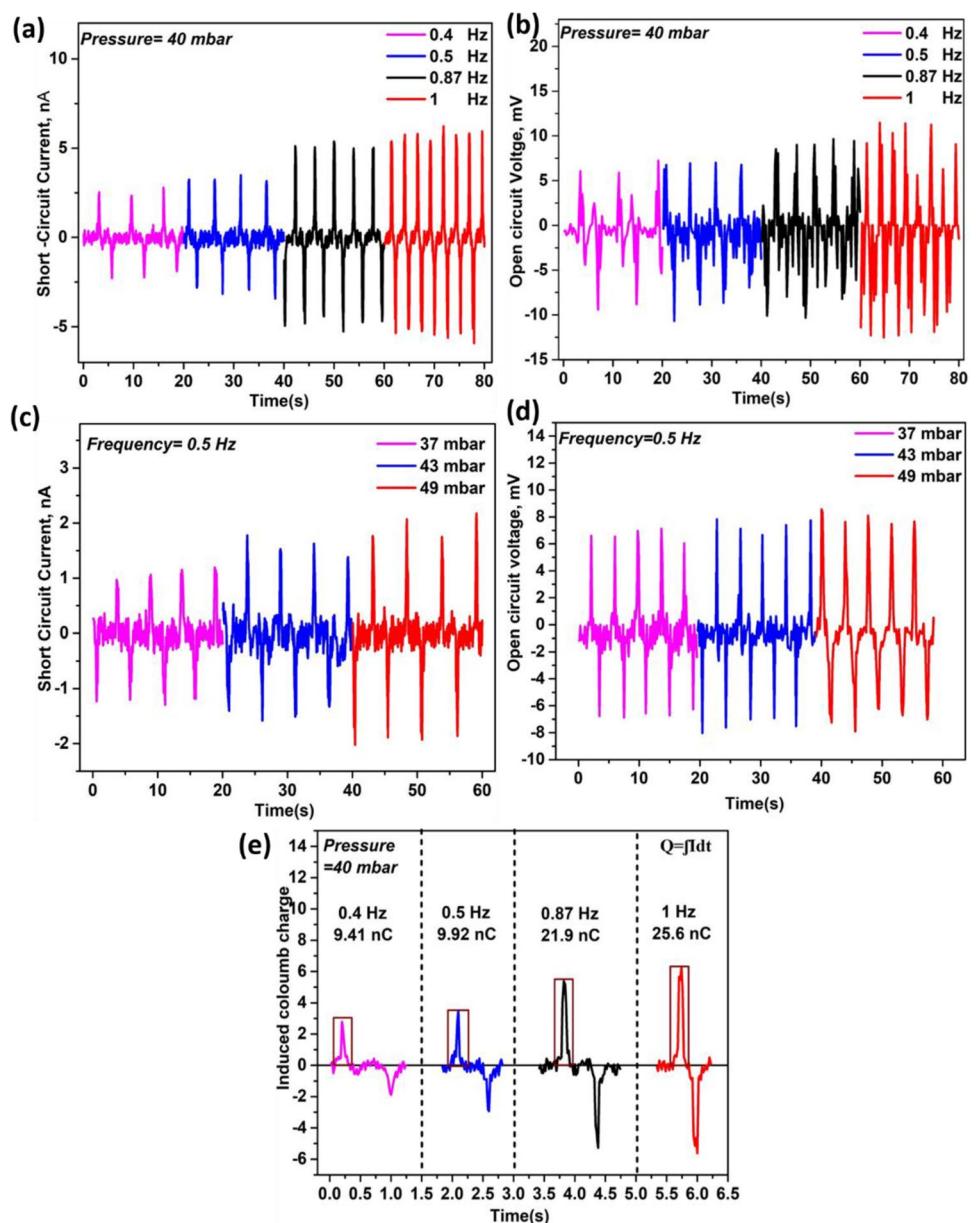
maintained like triangular amplitude to observe that the proposed DLC-TENG is instantaneously responsive to the sudden fluctuation of pressure. As shown in Fig. 4a, b, with the fixed pressure value of 40 mbar, the frequencies of the back and forth motion of the rotary oscillator were kept 0.4 Hz, 0.5 Hz, 0.87 Hz and 1 Hz. Under these resonance frequencies, the peak to peak short circuit current and open circuit voltage of the oscillating water column are 4.43 nA, 6.41 nA, 10.5 nA, 11.82 nA; 11.8 mV, 15.6 mV, 19.2 mV, 23.9 mV, respectively. From this observation, the uniform AC signal shows good performance with the increment of the frequency. For different pressure values applied with a frequency of 0.5 Hz, the output data was analyzed as depicted in Fig. 4c, d. The I_{sc} and V_{oc} (Peak to peak) for 37, 43 and 49 mbar are 2.33 nA; 3.27 nA; 3.97 nA, 13.56 mV; 15.42 mV; 15.58 mV, respectively. Though the voltage output was slightly varied when the pressure value changes from 43 and 49 mbar but the current values can be distinguished to be effectively utilized as a pressure sensor. The induced coulomb charges with 0.4, 0.5, 0.87 and 1 Hz are 9.41 nC; 9.92 nC; 21.9 nC; 25.6 nC, respectively and is shown in Fig. 4e. It is to be noted

that, the peak to peak I_{sc} and V_{oc} for each frequency and pressure value were analyzed over a definite time interval. As to quantify a triboelectric nanogenerator for the self-powered sensor, time is an essential factor. The generated I_{sc} and V_{oc} should be stable over a certain time period at the same parameter, otherwise the proposed system can't be regarded as a sensor.

The DLC-TENG performance was visualized by employing one PDMS channel in the experimental setup but varying the gap of the electrode. Figure 5a shows the I_{sc} of the 5 mm and 10 mm of a gap of the electrode while the discrete liquid column volume and position was kept fixed. For all frequencies, the DLC-TENG cell, with the 10 mm electrode gap between them shows better performance. As it can be explained that, with the reduction of the gap of the electrode, the water column moves back and forth very fast over the polymer surface, hence the water column doesn't have enough time interval for the charge to be induced consequently generates lower output. The prospect of the DLC-TENG as a frequency and pressure measurement device is illustrated in Fig. 5b, c respectively. The tendency of the curves is almost linear with frequency and pressure
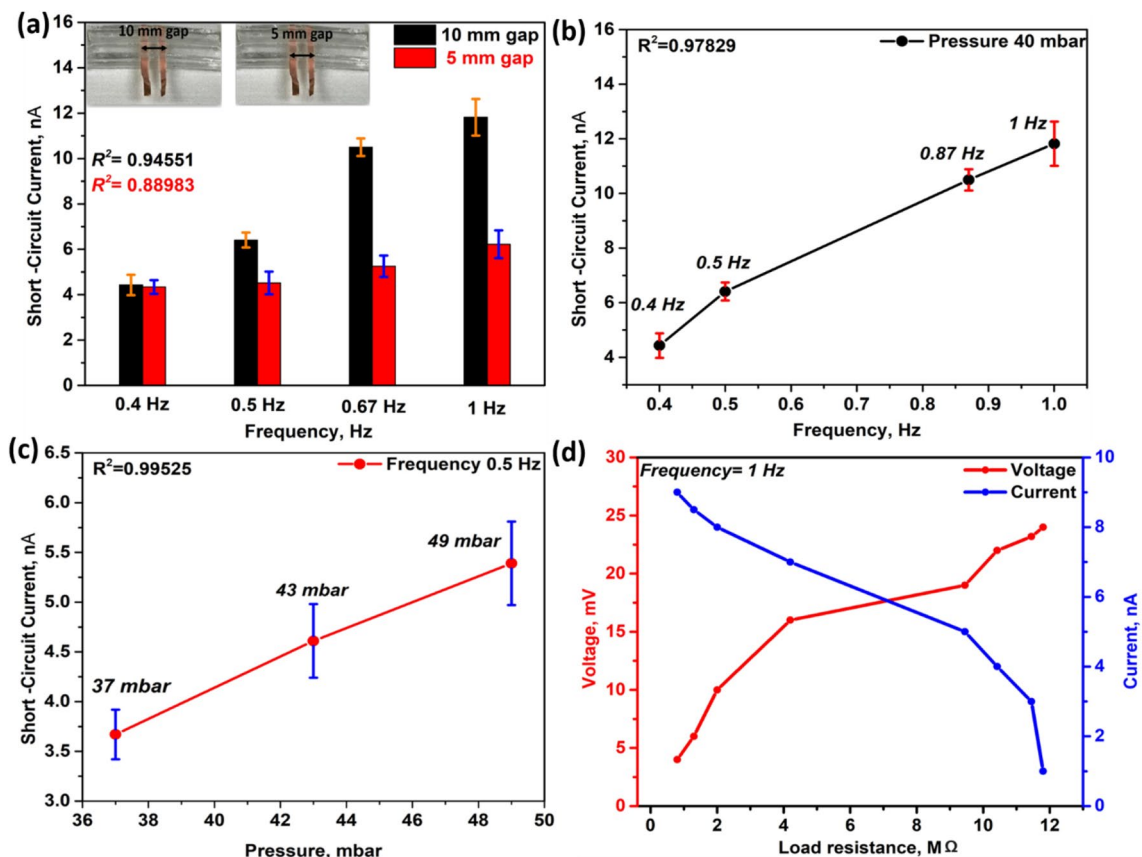
Fig. 5 **a** Short circuit current at the various frequency for 10 mm and 5 mm electrode gap. The linear increasing trend of the current curve with respect to the **b** frequency and **c** pressure variation response to be applied as a sensor. **d** At the frequency of the 1 Hz the voltage and current output against different load resistance

responses. Finally, to be realized as a self-powered device, the voltage and current were measured with respect to different load resistance at the frequency of 1 Hz as shown in Fig. 5d. The resistance was varied from the 0 to 12 MΩ and the maximum voltage of 25 mV and current of 9 nA were found at 12 MΩ and 1 MΩ respectively. From this observation, it is conspicuous that our proposed DLC-TENG can be effectively applied for the self-powered robust, flexible, cost-effective, easily fabricated transducer, where observing small scale change of physical properties is needed to be observed.

5 Conclusions

In summary, a regular AC output has obtained from the DLC-TENG to be effectively utilized for sensing applications and energy harvesting. The developed DLC-TENG with easy fabrication techniques is eco-friendly and portable. The proposed TENG is highly durable with lower volumes of injected liquid in the channel to generate the desirable consistent output of V_{oc} and I_{sc}. The mechanistic pathway evolved in the system based on free-standing sliding mode TENG from the cited previous reports has supported the generation of current and voltage. The surface morphology, checked by the FE-SEM, has proved the obvious structural change of the contact surface and further improved hydrophobicity has confirmed by the contact angle analysis. The DLC-TENG has shown sensible response to the different frequency and pressure values. Therefore, we expect that our self powered DLC-TENG would provide a simple way for possible application in various physical parameter sensing and detection.

References

1. Brown, K. S. (1999). Bright future-or brief flare-for renewable energy. *Science, 285,* 678–680.
2. Lund, H. (2007). Renewable energy systems. *Energy, 32,* 912–919.
3. Wang, Z. L., Jiang, T., & Xu, L. (2017). Toward the blue energy dream by triboelectric nanogenerator networks. *Nano Energy, 39,* 9–23.
4. Fan, F. R., Tian, Z. Q., & Wang, Z. L. (2012). Flexible triboelectric nanogenerator. *Nano Energy, 1,* 328–334.
5. Wang, Z. L. (2017). Catch wave power in floating nets. *Nature, 542,* 159–160.
6. Wang, Z. L. (2017). On Maxwell's displacement current for energy and sensors. *Materials Today, 20,* 74–82.
7. Wang, Z. L., Chen, J., & Lin, L. (2015). Progress in triboelectric nanogenerators as a new energy technology and self powered sensors. *Energy & Environmental Science, 8,* 2250–2282.
8. Zi, Y. L., & Wang, Z. L. (2017). Nanogenerators: an emerging technology towards nanoenergy. *Applied Physics Letters Materials, 5,* 074103.
9. Yang, X., Chan, S., Wang, L., & Doud, W. A. (2018). Water Tank triboelectric nanogenerator for efficient harvesting of water wave energy over a broad frequency range. *Nano Energy, 44,* 388–398.
10. Zhang, M., Jie, Y., Cao, X., Bian, J., Li, T., Wang, N., et al. (2016). Robust design of unearthed single-electrode TENG from three-dimensionally hybridized copper/polydimethylsiloxane film. *Nano Energy, 30,* 155–161.
11. Li, Z. L., Shen, J. L., Abdalla, I., & Yu, J. Y. (2017). Ding, B, Nanofibrous membane constructed wearable triboelectric nanogenerator for high performance biomechanical energy harvesting. *Nano Energy, 36,* 341–348.
12. Ahn, S.-H. (2014). An evaluation of green manufacturing technologies based on research databases. *International Journal of Precision Engineering and Manufacturing-Green Technology, 1*(1), 5–9.
13. Lee, D., Chung, J., Yong, H., Lee, S., & Shin, D. (2019). A deformable foam-layered triboelectric tactile sensor with adjustable dynamic range. *International Journal of Precision Engineering and Manufacturing-Green Technology, 6*(1), 43–51.
14. Lee, E. K., Yin, L., Lee, Y., Lee, J. W., Lee, S. J., Lee, J., et al. (2012). Large Thermoelectric figure-of-merits from SiGe nanowire by simultaneously measuring electrical and thermal transport properties. *Nano Letters, 12,* 2918.
15. Lee, J. H., Lee, Y. K., Gupta, M. K., Kim, T. Y., Lee, D. Y., Oh, J., et al. (2014). Highly stretchable piezoelectric-pyroelectric hybrid nanogenerator. *Advanced Materials, 26,* 765.
16. Yang, Y., Jung, J. H., Yun, B. K., Zhang, F., Pradel, K. C., et al. (2012). Flexible pyroelectric nanogenerators using a composite structure of lead-Free KNbO3 nanowires. *Advanced Materials, 24*(39), 5357–5362.
17. van der Heyden, F. H., Bonthuis, D. J., Stein, D., Meyer, C., & Dekker, C. (2007). Power generation by pressure-driven transport of ions in nanofluidic channels. *Nano Letters, 7*(4), 1022–1025.
18. van der Heyden, F. H., Stein, D., & Dekkar, C. (2005). Streaming current in a single nanofluidic channel. *Physical Review Letters, 95*(11), 116104.
19. Bae, J., Lee, J., Kim, S., Ha, J., Lee, B. S., et al. (2014). Flutter-driven triboelectrification for harvesting wind energy. *Nature Communications, 5,* 4929.
20. Wang, Li, S., Wen, Z., et al. (2016). Effective energy storage from a triboelectric nanogenerator. *Nature Communications, 7,* 10987.
21. Wang, Z. L. (2013). Triboelectric nanogenerators as new energy technology for self-powered systems and as active mechanical and chemical sensors. *ACS Nano, 7,* 9533–9557.
22. Lin, L., Xie, Y. N., Wang, S. H., Wu, W. Z., Niu, S. M., Wen, X. N., et al. (2013). Triboelectric active sensor array for self-powered static and dynamic pressure detection and tactile imaging. *ACS Nano, 7,* 8266–8274.
23. Yang, Y., Zhang, H., Lin, Z. H., Zhou, Y. S., Jing, Q., Su, Y., et al. (2013). Human Skin based triboelectric nanogenerators for harvesting biomechanical energy and as self-powered active tactile sensor system. *ACS Nano, 7,* 9213.
24. Zhu, G., Yang, W. Q., Zhang, T., Jing, Q., Chen, J., Zhou, Y. S., et al. (2014). Self-powered, ultrasensitive, flexible tactile sensors based on contact electrification. *Nano Letters, 14,* 3208.
25. Zhou, Y. S., Zhu, G., Niu, S., Liu, Y., Bai, P., Jing, Q., et al. (2014). Nanometer resolution self-powered static and dynamic

motion sensor based on micro-grated triboelectrification. *Advanced Materials, 26,* 1719.

26. Lin, Z. H., Zhu, G., Zhou, Y. S., Yang, Y., Bai, P., Chen, J., et al. (2013). A self-powered triboelectric nanosensor for mercury ion detection. *Angewandte Chemie, International Edition, 52,* 5065.

27. Li, Z., Chen, J., Yang, J., Su, Y., Fan, X., Wu, Y., et al. (2015). *β*-cyclodextrin enhanced triboelectrification for self-powered phenol detection and electrochemical degradation. *Energy & Environmental Science, 8,* 887–896.

28. McCarty, L. S., & Whitsides, G. M. (2008). Electrostatic charging due to separation of ions at interfaces: contact electrification of ionic electrets. *Angewandte Chemie, International Edition, 47,* 2188–2207.

29. Wiles, J. A., Grzybowski, W. A., & Whitesides, G. M. (2003). A tool for studying contact electrification in systems comprising metals and insulating polymers. *Analytical Chemistry, 75,* 4859–4867.

30. Lin, Z. H., Zhu, G., Zhou, S. Y., Yang, Y., Bai, P., Chen, J., et al. (2013). A self-powered triboelectric nanosensor for mercury ion detection. *Angewandte Chemie, International Edition, 52,* 5065–5069.

31. Chen, J., & Wang, Z. L. (2017). Reviving vibration energy harvesting and self-powered sensing by a triboelectric nanogenerator. *Joule, 1,* 480–521.

32. He, C., Han, C. B., Gu, G. Q., Jiang, T., Chen, B. D., Gao, Z. L., et al. (2017). Hourglass triboelectric nanogenerator as a "direct current" power source. *Advanced Energy Materials, 7,* 1700644.

33. Li, S. M., Wang, J., Peng, W. B., Lin, L., Zi, Y. L., Wang, S. H., et al. (2017). Sustainable energy source for wearable electronics based on multilayer elastomeric triboelectric nanogenerators. *Advanced Energy Materials, 7,* 1700644.

34. Fan, F. R., Lin, L., Zhu, G., Wu, W., Zhang, R., & Wang, Z. L. (2012). Transparent triboelectric nanogenerators and self-powered pressure sensors based on micropatterned plastic films. *Nano Letters, 12,* 3109–3114.

35. Nguyen, V., Zhu, R., & Yang, R. S. (2015). Environmentally Effects on Nanogenerators. *Nano Energy, 14,* 49–61.

36. Zhang, X. L., Zheng, Y. B., Wang, D. A., & Zhou, F. (2017). Solid-liquid triboelectrification in smart U tube for multifunctional sensors. *Nano Energy, 40,* 95–106.

37. Lin, Z.-H., Cheng, G., Lee, S., Pradel, K. C., & Wang, Z. L. (2014). Harvesting water drop energy by a sequential contact-electrification and electrostatic induction process. *Advanced Materials, 26,* 4690–4696.

38. Yang, J., & Kwok, D. Y. (2003). Microfluid flow in circular microchannel with electokinetic effect and Navier's slip condition. *Langmuir, 19*(4), 1047–1053.

39. Ren, Y., & Stein, D. (2008). Slip-enhanced electrokinetic energy conversion in nanofluidic channels. *Nanotechnology, 19*(19), 195707.

40. Choi, Y. W., Jang, S., Chun, M. S., Kim, S. M., & Choi, M. (2018). Efficient microfluidic power generator based on interaction between DI water and hydrophobic-channel surface. *International Journal of Precision Engineering and Manufacturing-Green Technology, 5*(2), 255–260.

41. Shi, Q., Wang, H., Wang, T., & Lee, C. (2016). Self-Powered liquid triboelectric microfluidic sensor for pressure sensing and finger motion monitoring applications. *Nano Energy, 30,* 450–459.

42. Jeon, S.-B., Seol, M.-K., Kim, D., Park, S. J., & Choi, Y.-K. (2016). Self-powerd ion concentration sensor with triboelectricity from liquid-solid. *Contact Electrification, 2,* 1600006.

43. Yang, Y., Park, J., Kwon, S., & Kim, Y. S. (2015). Fluidic active transducer for electricity generation. *Scientific Reports, 5,* 15695.

44. Tropmann, A., Tanguy, L., Koltay, P., Zengerle, R., & Riegger, L. (2012). completely superhydrophobic PDMS surfaces for microfluidics. *Langmuir, 28*(22), 8292–8295.

45. Feng, C., Zisheng, G., & Dongxu, L. (2007). Preparation of material surface structure similar to hydrophobic structure of lotus leaf. *Journal of Wuhan University of Technology-Mater Science Edition, 23*(4), 513–517.

46. Hartcher-OBrien, J., Evers, J., & Tempelman, E. (2019). Surface roughnress of 3D printed materials: comparing physical measurements and human perception. *Materials Today Communication, 19,* 300–305.

47. Eddings, A. M., Johnson, A. M., & Gale, K. B. (2008). Determining the optimal PDMS-PDMS bonding technique for microfluidics devices. *Journal of Micromechanics and Microengineering, 18,* 067001.

48. Choi, D., Kim, D. W., Yoo, D., Cha, J. K., La, M., & Kim, S. D. (2017). Spontaneous occurrence of liquid-solid contact electrification in nature: toward a robust triboelectric nanogenerator inspired by the natural lotus leaf. *Nano Energy, 36,* 250–259.

49. Lee, B. W., Orr, D. E. The Triboelectric Series, Alphalab Inc. http://www.alphalabinc.com/triboelectric-series/. Accessed 10 Jan 2019.

M. Shahriar received his B. Sc degree from Chittagong University of Engineering and Technology (CUET), Bangladesh in 2017. Now he is studying towards M. Sc degree in Mechanical Engineering in University of Ulsan (UOU), South Korea. His current research interests are Triboelectric nanogeneraror, development of biocompatible thin film, microfluidics system for smart sensing applications, soft actuator and fluid-structure interaction diagnosis.

Cong Phat Vo received the B.E degree in the Electrical and Electronic Engineering Technology and the M.Sc. degree in the Mechatronics Engineering from Ho Chi Minh City University of Technology and Education, Vietnam in 2013 and 2016, respectively. He is currently pursuing the Ph.D. degree with the School of Mechanical Engineering, University of Ulsan, Ulsan, Korea. His research interests include robotics, intelligent control, and renewable energy.

Kyoung Kwan Ahn received the B.S. degree in the Department of Mechanical Engineering from Seoul National University in 1990, the M. Sc. degree in Mechanical Engineering from Korea Advanced Institute of Science and Technology in 1992 and the Ph.D. degree from Tokyo Institute of Technology in 1999. He is currently a Professor in the School of Mechanical Engineering, University of Ulsan, Ulsan, Korea. His research interests are fluid based triboelectric nanogenerator, micro fluidic control system, design and control of smart actuator using the smart material, fluid power control and active damping control and renewable energy. He is an Editor of IJCAS, an Editorial Board of Renewable Energy, Actuators and Journal of Engineering.